Theoretical investigation of steric effects on the S1 potential energy surface of o-carborane-anthracene derivatives

FAHRİ ALKAN

Research Article

Theoretical investigation of steric effects on the S1 potential energy surface of o-carborane-anthracene derivatives

Fahri ALKAN*

Department of Nanotechnology Engineering, Faculty of Engineering, Abdullah Gül University, Kayseri, Turkey

Abstract: TDDFT scan calculations were performed for s-carborane-anthracene derivatives (o-CB-X-*Ant* where X=-H, -CH$_3$, -C$_2$H$_5$ and *tert*-butyl or -*t*Bu) in order to understand the interplay between the steric effects, S$_1$ potential energy surface (PES) and photophysical properties. The results show that all systems exhibit three local minima on the S$_1$ PES, which correspond to the emissive LE and TICT state, along with the nonemissive CT state respectively. In the case of the unsubstituted system (o-CB-H-*Ant*), and -CH$_3$ and -C$_2$H$_5$ substituted cases, S$_1$ PES is predicted to be quite flat for certain conformations indicating that it is possible for these systems to reach the nonemissive CT state without a large energy penalty. In comparison, conformational pathways for the nonemissive CT state are predicted to be energetically unfavorable for o-CB-*t*Bu-*Ant* as a result of both steric and electronic effects. These results provide a mechanism for the enhanced emission of σ-CB-fluorophore molecules with bulky ligands.

Key words: Carboranes, steric effects, excited-states, potential energy surface, TDDFT

1. Introduction

Icosahedral carborane clusters (C$_2$B$_{10}$H$_{12}$) show unique electronic and structural properties due to possessing three-center two electron bonds and s-aromaticity [1,2]. In recent years, significant progress has been made in C-H or B-H functionalization of carboranes, which enables carborane clusters to be employed as building blocks for nanoclusters, opto-electronic devices, and luminescent materials [3–6]. Among the possible isomers, σ-carborane (σ-CB) is the most widely-studied system due to its stability and relative ease of functionalization. In particular, σ-CB-fluorophore architecture has attracted interest due to its distinct photophysical properties such as aggregation-induced emission (AIE) and multiple photoluminescence [1,7–15].

As shown previously, σ-CB-fluorophores can exhibit dual emission in solution from locally-exited (LE) and twisted intramolecular charge transfer (TICT) states as a result of the conformational flexibility of σ-CB-fluorophore [16–20]. In the case of LE state, S$_1$→S$_0$ (or S$_0$→S$_1$) transition is localized on the p-conjugated fluorophore, while TICT state exhibits the extension of p-conjugation through mixing of LUMO orbitals from σ-CB and the fluorophore moieties [16,17]. It is also shown that the orbital mixing becomes symmetrically largest with the perpendicular arrangement of σ-CB's C-C bond (C$_1$-C$_2$) relative to the plane of fluorophore's p system, and energetically favorable with the elongation of the same C$_1$-C$_2$ bond [21,22].

In solution state, σ-CB-fluorophore systems generally show poor emission quantum yields, [1,7,23,24] which is often associated with the nonradiative decay path resulting from the vibrational motion of C$_1$-C$_2$ bond [25,26]. More recently, it is shown that a nonemissive and energetically favorable charge-transfer (CT) state occurs on the S$_1$ potential energy surface (PES) of σ-CB-fluorophore systems as a result of significant C$_1$-C$_2$ bond elongation, which can also be a major pathway for nonradiative decay [22,27]. In comparison, the emission is shown to be recovered in solid state systems (AIE), or via structural limitations on C$_1$-C$_2$ bond elongation [9,16,18,28–35]. It should also be noted that enhanced emission quantum yields have been obtained in solution for σ-CB-fluorophore molecules when bulky ligands are introduced to the adjacent carbon of σ-CB [12,17,26,36–39]. However, the mechanism for this enhanced emission and the effect of steric hindrance on the electronic structure and excited state properties of such systems have not been fully explored using theoretical tools.

In this contribution, a detailed investigation for the S$_1$ PES of σ-CB-anthracene derivatives (o-CB-X-*Ant* where X=-H, -CH$_3$, -C$_2$H$_5$ and *tert*-butyl or -*t*Bu) is presented to understand the steric effects on the photophysical properties of σ-CB-

646

fluorophore molecules. The results show that while the nonemissive CT state is energetically favorable for *o*-CB-H-*Ant*, emissive TICT state becomes significantly more favorable with -*t*Bu substitution. It is also shown that energy barriers on S_1 PES for the conformations exhibiting parallel orientation of C_1-C_2 bond and *Ant* are quite large with -*t*Bu substitution compared to the cases in X =-H, -CH$_3$ and -C$_2$H$_5$. These findings provide a possible mechanism for the enhanced emission of σ-CB-fluorophore molecules with bulky ligands.

2. Materials and methods

All DFT and TDDFT computations were performed with Gaussian09 program package [40] using M06-2X [41] functional and 6-31g(d) basis set. In previous work, M06-2X functional is shown to provide better agreement with experiment for geometries and excited state properties compared to other functionals [22,42]. In addition, benchmark calculations on *o*-CB-H-*Ant* system with 6-311g(d) basis set were performed. It is seen that exited state energies differ only by 0.06–0.03 eV for LE, TICT, and CT states, indicating that 6-31g(d) provide sufficient accuracy for these systems. For TDDFT scan calculations, excited-state geometry optimizations were performed with constraints on C_1-C_2 bond length, and the dihedral angle between C_1-C_2 bond and the plane of *Ant* moiety, which are illustrated in Figure 1. Excited-state density differences and L values, which quantify the overlap between electron and hole wavefunctions for an excited state, were calculated using Multiwfn [43] program.

Solvent effects were considered with THF as solvent within the polarizable continuum formalism. In previous work, [44] solvent effects are shown to be small but noticeable for photophysical properties of σ-CB-fluorophore systems. In that aspect, benchmark calculations were performed for *o*-CB-H-*Ant* with toluene and acetonitrile as solvents in addition to THF. It is seen that while solvent effects are somewhat smaller (~0.05 eV) for the LE state, TICT and CT states become considerably stable (~0.2 eV) with acetonitrile as solvent compared to the case with toluene due to charge transfer nature of the excited states.

3. Results and discussion

Figure 2 shows the optimized ground state geometries, and the frontier energy levels which contribute significantly to the excited-state dynamics for *o*-CB-X-*Ant*. For ground state geometries, *o*-CB-H-*Ant* exhibits a -15° dihedral angle (φ), whereas the substituted systems (*o*-CB-CH$_3$-*Ant*, *o*-CB-C$_2$H$_5$-*Ant* and *o*-CB-*t*Bu-*Ant*) exhibit tilted φ ranging between –86° and –88°. This result originates from the fact that steric effects are quite substantial even with the -CH$_3$ substitution for small φ and unstretched C_1-C_2 bond. It is seen that both HOMO and LUMO levels are mainly localized on the *Ant* moiety, while LUMO+2 level exhibits significant contribution from *o*-CB in all cases. It should also be noted that the LUMO+2 level exhibits large antibonding character on the C_1-C_2 bond. As a result, this level is shown to undergo significant stabilization with increasing C_1-C_2 bond length and ordering of LUMO and LUMO+2 can be altered upon excitation induced geometry change [22,27].

In Table 1, the excited state energetics, oscillator strengths, and geometric parameters for vertical 0→1 transition (absorption), along with 1→0 transitions (emission) for LE, TICT, and CT states are tabulated. The geometries show only
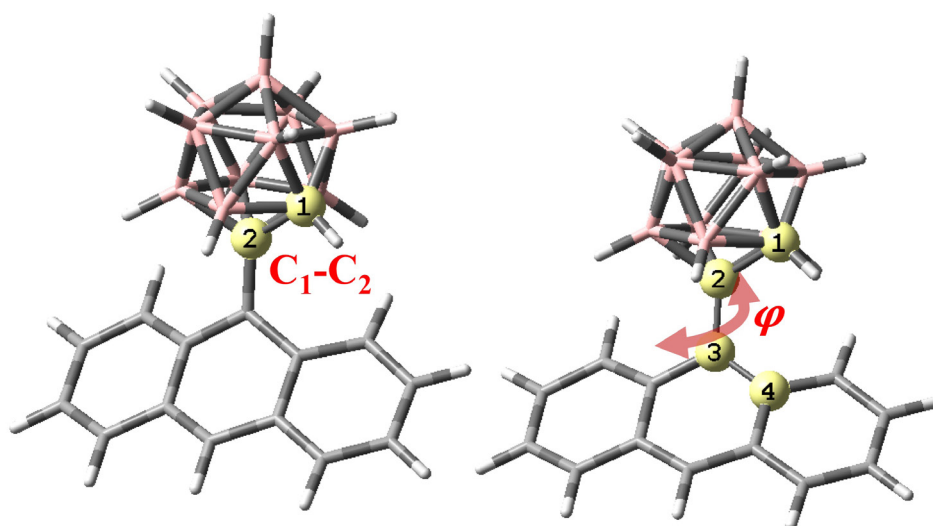

Figure 1. Illustration of C_1-C_2 bond length and the dihedral angle (φ) between C_1-C_2 bond and the plane of *Ant* moiety (C_1-C_2-C_3-C_4) for *o*-CB-X-*Ant*.
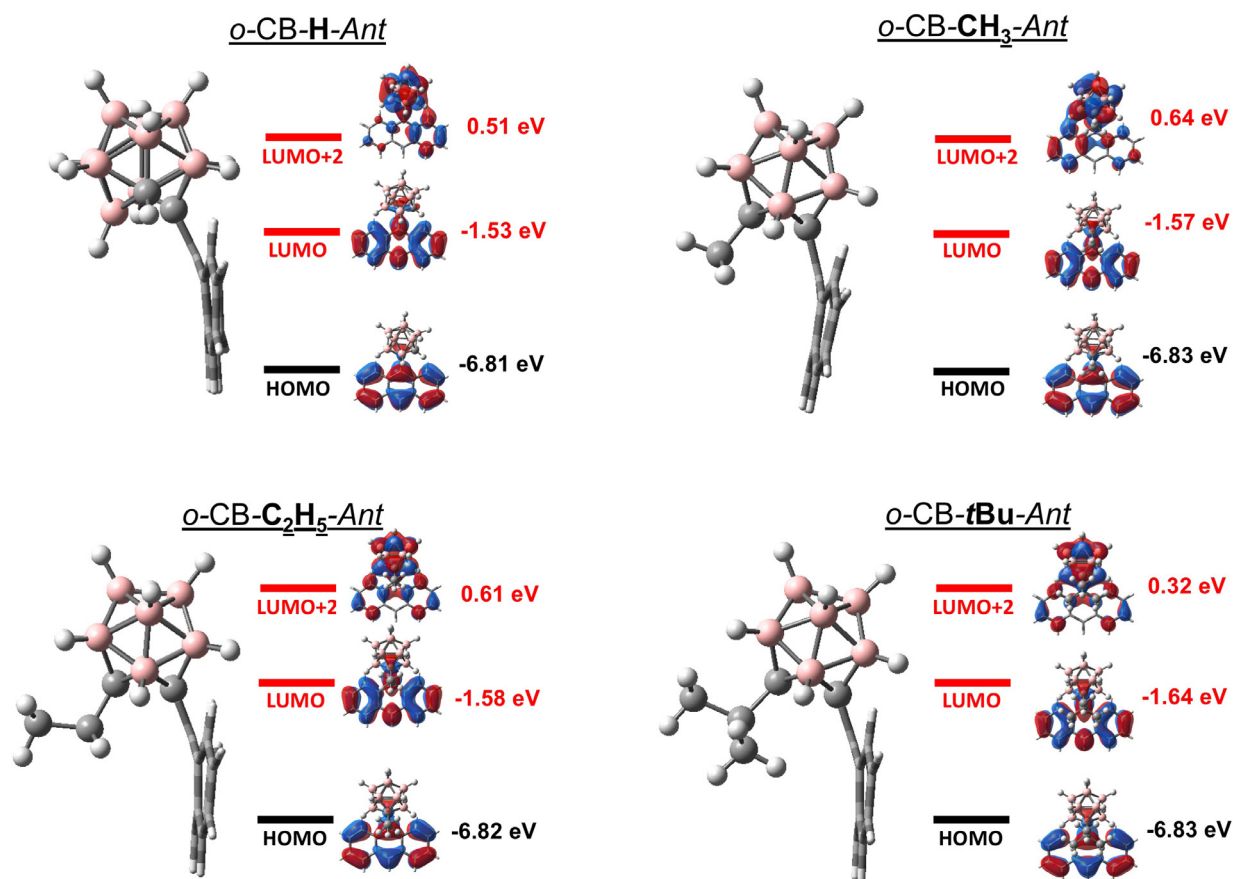
Figure 2. Ground state geometries and selected energy levels for σ-CB-anthracene derivatives.

slight changes from the ground-state geometries for the 1→0 transitions of LE state. Regardless of this slight conformational change, both 0→1 transitions and 1→0 transitions in LE state originate from local π-π* transitions on the *Ant* moiety for all systems, while the contribution from *o*-CB is minimal. As a result, calculated oscillator strengths and energies (*f*) show quite similar values due to similar nature of the transition for these systems.

For the case of TICT state, it is previously shown that *o*-CB-H-*Ant* undergoes to a rotation with respect to *φ*, along with C_1-C_2 bond elongation compared to the LE or S_0 states [16]. For the substituted systems, the conformations for TICT state also exhibit a tilted *φ* and partially elongated C_1-C_2 bonds. The elongation of C_1-C_2 bond is slightly less for *o*-CB-CH$_3$-*Ant* and *o*-CB-C$_2$H$_5$-*Ant* (2.11 and 2.14 Å respectively), while the same bond length becomes substantially larger for *o*-CB-*t*Bu-*Ant* (2.35 Å). Furthermore, TICT state of *o*-CB-*t*Bu-*Ant* shows significant stabilization (0.31 eV) for the adiabatic energy (E_{S1}) compared to LE state. In comparison, calculated E_{S1} is quite comparable for LE and TICT states of other molecules. In all cases, TICT state exhibits an increase for the contribution of *o*-CB moiety to electron wavefunction along with an increase for the oscillator strengths showing hybridized local and charge transfer (HLCT) character.

In our recent work, it is seen that significant elongation of C_1-C_2 bond and parallel orientation between two moieties (*φ* = 0°) result in a nonemissive CT state for *o*-CB-H-*Ant*.[22] Furthermore, this CT state is shown to be the global minimum for the S_1 PES, which suggests that it can be an important pathway for fluorescence quenching. A similar dark CT state is also found for all substituted systems as shown in Table 1. In the case of *o*-CB-CH$_3$-*Ant* and *o*-CB-C$_2$H$_5$-*Ant*, C_1-C_2 bond length becomes 2.59 Å for the dark CT state, while the same C_1-C_2 bond becomes even more elongated for *o*-CB-*t*Bu-*Ant* (2.68 Å), which most likely results from the steric hindrance of bulky -*t*Bu group. Another important point is that while the E_{S1} of the CT state is ~0.2 eV lower compared to the E_{S1} of the TICT state of *o*-CB-H-*Ant*, the same CT state is energetically less favorable (~0.2 eV) in the case of *o*-CB-*t*Bu-*Ant*. For *o*-CB-CH$_3$-*Ant* and *o*-CB-C$_2$H$_5$-*Ant*, the energy differences between two states are less pronounced for these systems compared to the cases in *o*-CB-*t*Bu-*Ant* or *o*-CB-H-*Ant*.

Table 1. Comparison of 0→1 or 1→0 transition energies, oscillator strengths, energy difference between the ground state and excited state geometries (ΔE_0), adiabatic excited state energies (ES_1), and geometrical parameters of each conformation for o-CB-Ant derivatives.

o-CB-fluorophore	0→1 or 1→0 (eV)	Oscillator Strength (a.u)	ΔE_0 (eV)	E_{S1} (eV)	C_1-C_2 length (Å)	φ C_1-C_2-C_3-C_4 (degrees)
Vertical transition (0*1)						
o-CB-H-*Ant*	3.37	0.22	0.00	3.37	1.65	-15
o-CB-CH$_3$-*Ant*	3.33	0.21	0.00	3.33	1.71	-86
o-CB-C$_2$H$_5$-*Ant*	3.28	0.27	0.00	3.28	1.73	-87
o-CB-*t*Bu-*Ant*	3.28	0.22	0.00	3.28	1.80	-88
LE State (1*0)						
o-CB-H-*Ant*	2.61	0.25	0.36	2.97	1.66	-13
o-CB-CH$_3$-*Ant*	2.55	0.24	0.39	2.94	1.71	-86
o-CB-C$_2$H$_5$-*Ant*	2.55	0.21	0.37	2.92	1.72	-86
o-CB-*t*Bu-*Ant*	2.56	0.26	0.34	2.90	1.80	-88
TICT State (1*0)						
o-CB-H-*Ant*	2.25	0.49	0.72	2.97	2.25	-86
o-CB-CH$_3$-*Ant*	2.31	0.38	0.54	2.85	2.11	-85
o-CB-C$_2$H$_5$-*Ant*	2.30	0.39	0.53	2.84	2.14	-86
o-CB-*t*Bu-*Ant*	2.19	0.49	0.40	2.59	2.35	-86
CT State (1*0)						
o-CB-H-*Ant*	1.31	0.00	1.48	2.79	2.53	0
o-CB-CH$_3$-*Ant*	1.23	0.00	1.63	2.87	2.59	0
o-CB-C$_2$H$_5$-*Ant*	1.24	0.00	1.66	2.89	2.59	0
o-CB-*t*Bu-*Ant*	1.13	0.00	1.68	2.81	2.68	0

To further understand the steric effects on the photophysical properties of *o*-CB-X-*Ant* systems, the PESs of the S$_1$ state are scanned with respect to C$_1$-C$_2$ bond length and φ. In Figure 3a and 3b, the results are shown for conformations with varying C$_1$-C$_2$ bond length, and fixed φ (–90° and 0°) respectively. For the tilted geometries (φ = –90°), elongation of C$_1$-C$_2$ bond results in relatively flat PESs for the 1.7–2.4 Å range in the case of *o*-CB-H-*Ant* as shown in Figure 3a. Similar results are seen for the substituted systems when X = -CH$_3$ and -C$_2$H$_5$. For the latter, calculated E$_{S1}$ shows an increase with further elongation of C$_1$-C$_2$ bond beyond 2.4 Å. In comparison, the PES of *o*-CB-*t*Bu-*Ant* shows a clear minimum between 2.3–2.4 Å, which roughly corresponds to the TICT (φ = –86°) state shown in Table 1. In this case, elongation of C$_1$-C$_2$ bond results in a decrease for E$_{S1}$ for the 1.7–2.4 Å range, which arises from the steric strain relaxation of bulky -*t*Bu group.

For parallel geometries (φ = 0°), lowest energy points for the calculated E$_{S1}$ are found with conformations showing fully elongated C$_1$-C$_2$ bond lengths, which also correspond to the dark CT states of these systems as shown in Table 1. For *o*-CB-H-*Ant*, PES shows an energy barrier of ~0.4 eV, where the local maximum is located at 2.1 Å. This is also the case for *o*-CB-CH$_3$-*Ant* and *o*-CB-C$_2$H$_5$-*Ant*, however, the calculated energy barriers are somewhat smaller (~ 0.1 eV) with respect to shorter C$_1$-C$_2$ bonds. It should be noted that the steric effects are more pronounced for parallel conformations (φ = 0°) due to the alignment of -X group with anthracene moiety, and these steric effects mostly dominate the excited-state energetics for relatively short C$_1$-C$_2$ bonds. In fact, the most drastic result is seen for X = -*t*Bu case, for which the PES shows a large destabilization of E$_{S1}$ as shown in Figure 3b. For this system, PES does not exhibit an energy barrier since calculated E$_{S1}$ becomes continuously more stable with elongation of the C$_1$-C$_2$ bond.

In addition to the excited-state energetics, it is important to assess the nature of S$_1$→S$_0$ transitions on the PESs to fully understand the photophysical processes and the origin of energy barriers. In Figure 4a and 4b, calculated Λ values, which quantify the overlap degree ($0 \leq \Lambda \leq 1$) between electron and hole wave functions [45], are illustrated for the S$_1$→S$_0$ transitions of tilted (φ = –90°) and parallel conformations (φ = 0°) with respect to C$_1$-C$_2$ bond lengths. For both φ, S$_1$→S$_0$ transitions mainly originate from local π-π^* transition on the anthracene moiety, and show LE character for shorter C$_1$-
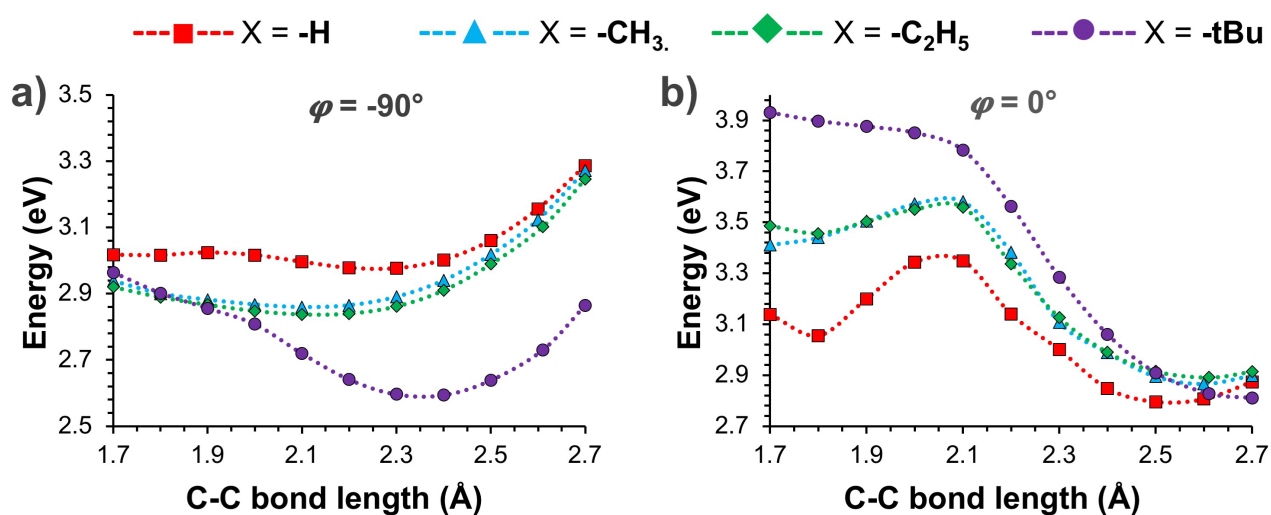
Figure 3. Calculated PESs for the S_1 state of *o*-CB-X-*Ant* systems with respect to varying C_1-C_2 bond length, and fixed *j* at a) −90° and b) 0°.
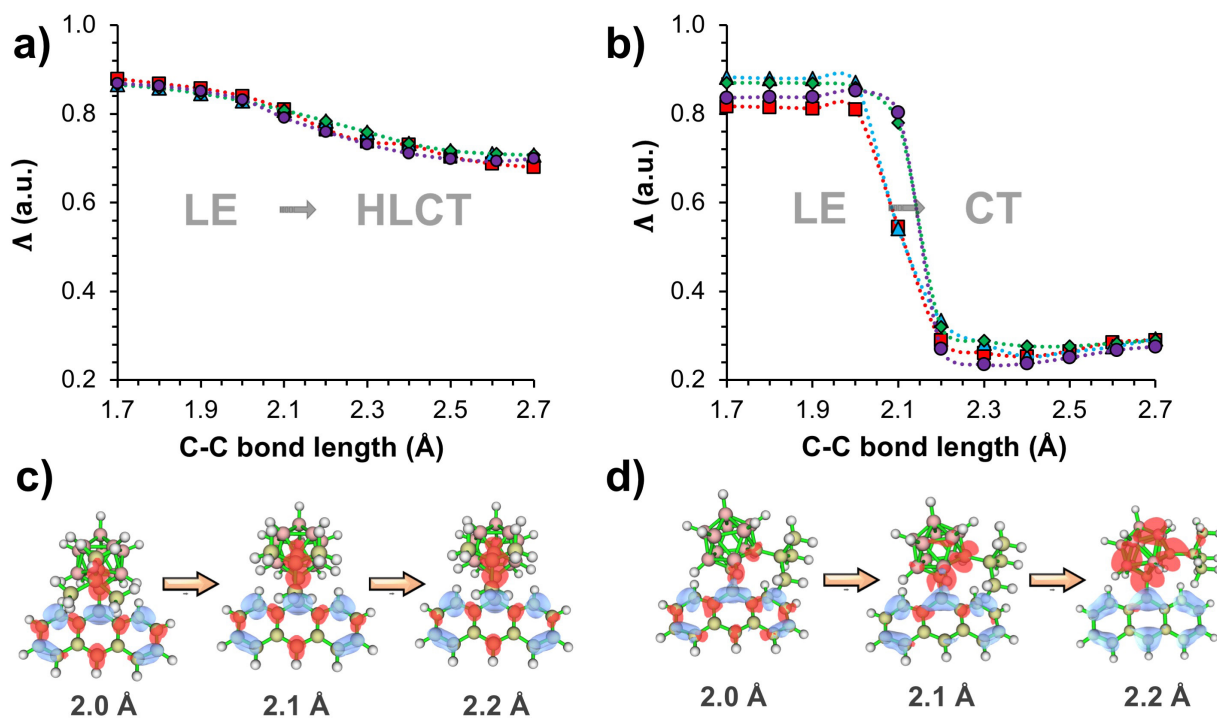

Figure 4. Calculated L values for a) tilted (*j* = −90°) and b) parallel conformations (*j* = 0°) with respect to C_1-C_2 bond lengths, and illustrations of excited-state density differences for c) tilted and d) parallel conformations at 2.0, 2.1, and 2.2 Å C_1-C_2 bond length.

C_2 bond lengths with Λ larger than 0.8. In the case of tilted geometries, calculated Λ values become continuously smaller with increasing C_1-C_2 bond lengths, indicating more HLCT character for the $S_1 \rightarrow S_0$ transitions of all systems. This result originates from the larger *o*-CB character for the electron wave function with elongated C_1-C_2 bond lengths. This effect is also illustrated with excited-state density differences shown in Figure 4c for *o*-CB-*t*Bu-*Ant*. As the C_1-C_2 bond length elongates from 2.0 Å to 2.2 Å, electron density (shown as red) on *o*-CB gradually increases showing CT from *Ant* to *o*-CB
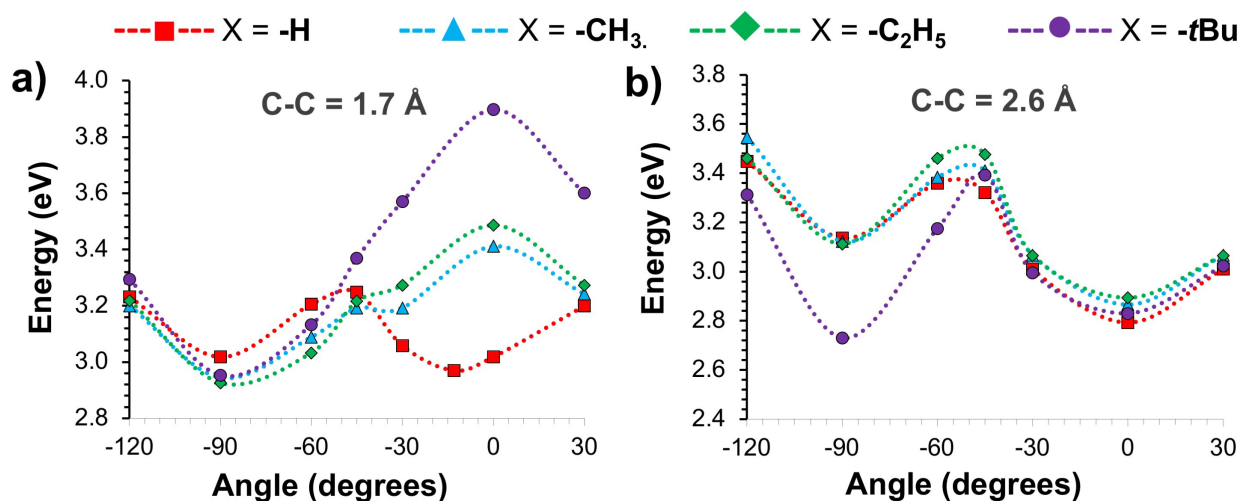
Figure 5. Calculated PESs for the S$_1$ state of *o*-CB-X-*Ant* systems with respect to varying *j*, and fixed C$_1$-C$_2$ bond length at a) 1.7 Å and b) 2.6 Å.

upon excitation. Meanwhile, there is also considerable hole (shown as blue) and electron density on *Ant*, which indicates the presence of local π-π* character for the overall excited state nature.

For parallel conformations (φ = 0°), calculated Λ values (0.8–0.9) also exhibit LE character for the S$_1$→S$_0$ transitions when the C$_1$-C$_2$ bond length is within 1.7–2.1 Å. At 2.1 Å, however, the nature of S$_1$→S$_0$ transitions drastically transform to CT character as indicated from the sharp decrease of Λ values. This effect is also evident from excited-state density differences shown in Figure 4d. While electron and hole densities are mainly localized on *Ant* moiety when the C$_1$-C$_2$ bond length is 2.0 Å, they show a strong charge separation when C$_1$-C$_2$ bond length is 2.2 Å. It should also be noted that PESs (Figure 2b) show a significant decreasing trend for the calculated E$_{S1}$ of all systems at 2.1 Å bond length, which is initiated with the LE→CT transformation of S$_1$→S$_0$ transitions.

Similar to the C$_1$-C$_2$ bond elongation, the PESs of the S$_1$ states are also scanned with respect to *j* for selected bond lengths (1.7 or 2.6 Å). The results are illustrated in Figure 5a and 5b, respectively.

For the unsubstituted system, calculated PES shows two local minima with respect to *j* ($\varphi \approx$ –90° and $\varphi \approx$ –13°) when the C$_1$-C$_2$ bond length is 1.7 Å. In comparison, PESs of substituted systems exhibit only one local minimum at φ » –90°, whereas $\varphi \approx$ 0° corresponds to the maxima for these cases. This energy penalty for the S$_1$ stated at $\varphi \approx$ 0° results from steric effects, which is significantly larger for the bulky -*t*Bu group as shown in Figure 5a. For these conformations, S$_1$→S$_0$ transitions show LE character (π-π* transition on the anthracene moiety) for all systems regardless of φ in all cases as indicated by calculated Λ values and excited state density differences as shown in Figure 6a and 6c. As a result, excited state energetics are governed mainly by the steric hindrance of the bulky group rather than electronic effects for these conformations.

For conformations with fully elongated C$_1$→C$_2$ bond (2.6 Å), S$_1$ PESs show quite similar trends for both substituted and unsubstituted systems (Figure 5b) unlike the PESs with unstretched C$_1$→C$_2$. This is related to the reduction of steric hindrance on the molecular geometries with C$_1$-C$_2$ bond elongation. As shown in Figure 5b, two local minima ($\varphi \approx$ -90° and $\varphi \approx$ 0°) exist in the PESs for all systems, which correspond S$_1$→S$_0$ transitions with HLCT and CT characters (Figures 6b and 6d) respectively. With -CH$_3$ and -C$_2$H$_5$ substitution as well as with the unsubstituted system, parallel conformation (φ = 0°) is predicted to be energetically more favorable compared to the tilted conformation (φ = 90°), whereas tilted conformation is still energetically more favorable with -*t*Bu substitution. In addition, the rotational energy barrier is significantly larger with -*t*Bu substitution (~0.7 eV)), indicating a less probable path for the formation of dark CT state for this case.

In previous experimental and theoretical studies, it is shown that *o*-CB-H-*Ant* exhibits dual emission in solution from energetically close LE and TICT conformations on S$_1$ PES [16]. However, experimentally obtained quantum yield of the florescence is quite low in solution (Φ_{PL} = 0.02), which is associated with quenching through low-energy dark CT state [22,27], along with the vibrational motion of C$_1$-C$_2$ bond on *o*-CB. [32] Correspondingly, a single emission band with low quantum yield (Φ_{PL} < 0.01) is found previously for *o*-CB--CH$_3$-*Ant* in solution state. In the case of bulky substituents such as -TMS (trimethylsilyl) or -*t*Bu, however, a significant increase for the quantum yield is observed for *o*-CB-*Ant* or other
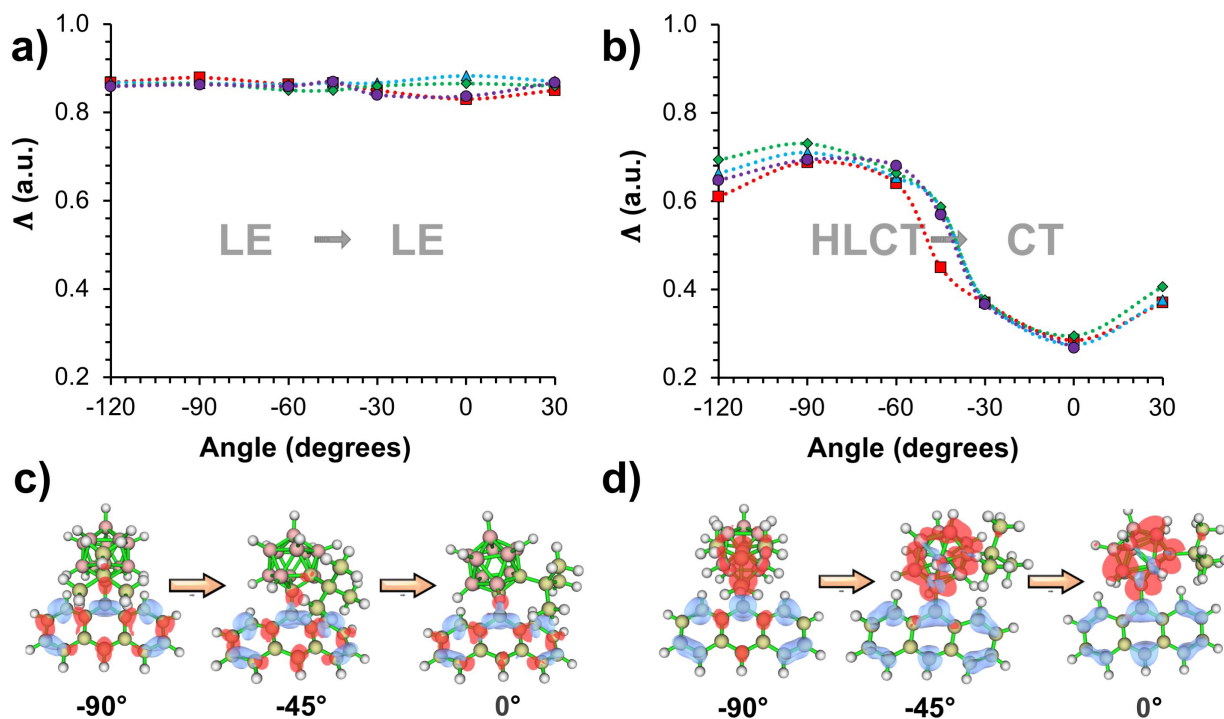
Figure 6. Calculated Λ values with varying *j* for conformations with a) unstretched (C_1-C_2 = 1.7 Å) and b) fully stretched (C_1-C_2 = 2.6 Å) C_1-C_2 bonds, and illustrations of excited-state density differences for c) unstretched and d) fully stretched conformations at –90°, –45°, and 0° dihedral angles.

o-CB-*fluorophore* systems [12,17,38]. The increase in the emission quantum yield is often associated to the suppression of C_1-C_2 vibrational motion as a result of steric effects induced by bulky groups. In this investigation, it is shown that the S_1 PESs of *o*-CB-*t*Bu-*Ant* exhibit distinct features compared to the unsubstituted or -CH_3 and -C_2H_5 substituted systems. One main difference is that the excited-state energies of parallel conformations ($\varphi \approx 0°$) with relatively short C_1-C_2 bonds are significantly higher for *o*-CB-*t*Bu-*Ant* compared to other systems. For these geometries, calculated E_{S1} also surpasses the initial excitation energy (E_{0*1}) for *o*-CB-*t*Bu-*Ant*, indicating energetically inaccessible conformations on S_1 PES.

Another important feature is that the twisted conformations ($\varphi \approx -90°$) are energetically more favorable for -*t*Bu substituted system, especially for 2.2–2.6 Å C_1-C_2 bond range. As a result, twisted conformation is predicted to be the minima for *o*-CB-*t*Bu-*Ant* even at 2.6 Å C_1-C_2 bond length, meanwhile parallel conformations (dark CT state) are predicted to be the minima for the other systems with the same C_1-C_2 bond length. It should also be noted that the CT state of the *o*-CB-H-*Ant* is predicted to be the global minimum on the S_1 PES, while CT state of *o*-CB-CH_3-*Ant* and *o*-CB-C_2H_5-*Ant* are within 0.05 eV with the TICT state of the same systems. Meanwhile, the difference between TICT and CT states of *o*-CB-*t*Bu-*Ant* is 0.22 eV, where the TICT conformation is predicted to be the global minimum on the S_1 PES. These results show that there is a substantial energy penalty for *o*-CB-*t*Bu-*Ant* to reach the parallel conformations and resulting dark CT state, which most likely constrain the molecule in the emissive twisted conformations.

4. Conclusion

In this contribution, TDDFT calculations were performed for the S_1 PES of *o*-CB-H-*Ant*, *o*-CB-CH_3-*Ant*, *o*-CB-C_2H_5-*Ant*, and *o*-CB-*t*Bu-*Ant* to understand the steric effects on the photophysical properties of *o*-CB-fluorophore systems. It is shown that a nonemissive CT state exists for all systems as a result of C_1-C_2 bond elongation (2.53–2.68 Å) and parallel orientation ($\varphi \approx 0°$) between two moieties. In the case of unsubstituted system (*o*-CB-H-*Ant*), the adiabatic energy of this CT state is lowest on the S_1 PES, whereas the CT state shows similar energetics with the emissive TICT state ($\varphi \approx -90°$) for -CH_3 and -C_2H_5 substituted cases. For these systems, it is seen that S_1 PES is predicted to be quite flat for conformations especially for tilted conformations, indicating that it is possible for these systems to reach the nonemissive CT state without a large energy penalty.

In comparison, S_1 PES of *o*-CB-*t*Bu-*Ant* clearly shows a global minimum for the conformations with $\varphi \approx -90°$ (TICT state), and the energy difference between the TICT and CT states are quite large (0.22 eV) with former being energetically favorable. In addition, adiabatic energies are significantly higher for parallel conformations ($\varphi \approx 0°$) of *o*-CB-*t*Bu-*Ant* compared to the initial vertical excitation energy (absorption), especially for shorter C_1-C_2 bonds. These results show that both pathways for the nonemissive CT state are energetically unfavorable for *o*-CB-*t*Bu-*Ant* as a result of the interplay between steric and electronic effects, which results in higher emission yields even in solution state.

References

1. Nunez R, Tarres M, Ferrer-Ugalde A, de Biani FF, Teixidor F. Electrochemistry and Photoluminescence of Icosahedral Carboranes, Boranes, Metallacarboranes, and Their Derivatives. Chemical Reviews 2016; 116 (23): 14307–14378. https://doi.org/10.1021/acs.chemrev.6b00198

2. Grimes RN. *Carboranes*. 3rd ed. Amsterdam: Academic Press; 2016.

3. Quan YJ, Xie ZW. Controlled functionalization of o-carborane via transition metal catalyzed B-H activation. Chemical Society Reviews 2019; 48 (13): 3660–3673. https://doi.org/10.1039/c9cs00169g

4. Qiu ZZ, Xie ZW. A Strategy for Selective Catalytic B-H Functionalization of o-Carboranes. Accounts of Chemical Research 2021; 54 (21): 4065–4079. https://doi.org/10.1021/acs.accounts.1c00460

5. Au YK, Xie ZW. Recent Advances in Transition Metal-Catalyzed Selective B-H Functionalization of o-Carboranes. Bulletin of the Chemical Society of Japan 2021; 94 (3): 879–899. https://doi.org/10.1246/bcsj.20200366

6. Ozcelik S, Gul A. Boron-containing tetrapyrroles. Turkish Journal of Chemistry 2014; 38 (6): 950–979. https://doi.org/10.3906/kim-1405-20

7. Ochi J, Tanaka K, Chujo Y. Recent Progress in the Development of Solid-State Luminescent o-Carboranes with Stimuli Responsivity. Angewandte Chemie-International Edition 2020; 59 (25): 9841–9855. https://doi.org/10.1002/anie.201916666

8. Marfavi A, Kavianpour P, Rendina LM. Carboranes in drug discovery, chemical biology and molecular imaging. Nature Reviews Chemistry 2022; 6 (7): 486–504. https://doi.org/10.1038/s41570-022-00400-x

9. Tominaga M, Naito H, Morisaki Y, Chujo Y. Colour-tunable aggregation-induced emission of trifunctional o-carborane dyes. New Journal of Chemistry 2014; 38 (12): 5686–5690. https://doi.org/10.1039/c4nj00955j

10. Cho YJ, Kim SY, Cho M, Han WS, Son HJ et al. Aggregation-induced emission of diarylamino-pi-carborane triads: effects of charge transfer and pi-conjugation. Physical Chemistry Chemical Physics 2016; 18 (14): 9702–9708. https://doi.org/10.1039/c5cp07883k

11. Furue R, Nishimoto T, Park IS, Lee J, Yasuda T. Aggregation-Induced Delayed Fluorescence Based on Donor/Acceptor-Tethered Janus Carborane Triads: Unique Photophysical Properties of Nondoped OLEDs. Angewandte Chemie-International Edition 2016; 55 (25): 7171–7175. https://doi.org/10.1002/anie.201603232

12. Naito H, Nishino K, Morisaki Y, Tanaka K, Chujo Y. Highly-efficient solid-state emissions of anthracene-o-carborane dyads with various substituents and their thermochromic luminescence properties. Journal of Materials Chemistry C 2017; 5 (38): 10047–10054. https://doi.org/10.1039/c7tc02682j

13. Jin GF, Cho YJ, Wee KR, Hong SA, Suh IH et al. BODIPY functionalized o-carborane dyads for low-energy photosensitization. Dalton Transactions 2015; 44 (6): 2780–2787. https://doi.org/10.1039/c4dt03123g

14. Kim SY, Cho YJ, Jin GF, Han WS, Son HJ et al. Intriguing emission properties of triphenylamine-carborane systems. Physical Chemistry Chemical Physics 2015; 17 (24): 15679–15682. https://doi.org/10.1039/c5cp01658d

15. Wee KR, Han WS, Cho DW, Kwon S, Pac C et al. Carborane Photochemistry Triggered by Aryl Substitution: Carborane-Based Dyads with Phenyl Carbazoles. Angewandte Chemie-International Edition 2012; 51 (11): 2677–2680. https://doi.org/10.1002/anie.201109069

16. Naito H, Nishino K, Morisaki Y, Tanaka K, Chujo Y. Solid-State Emission of the Anthracene-o-Carborane Dyad from the Twisted-Intramolecular Charge Transfer in the Crystalline State. Angewandte Chemie-International Edition 2017; 56 (1): 254–259. https://doi.org/10.1002/anie.201609656

17. Weber L, Kahlert J, Brockhinke R, Bohling L, Brockhinke A et al. Luminescence Properties of C-Diazaborolyl-ortho-Carboranes as Donor-Acceptor Systems. Chemistry-a European Journal 2012; 18 (27): 8347–8357. https://doi.org/10.1002/chem.201200390

18. Wee KR, Cho YJ, Song JK, Kang SO. Multiple Photoluminescence from 1,2-Dinaphthyl-ortho-Carborane. Angewandte Chemie-International Edition 2013; 52 (37): 9682–9685. https://doi.org/10.1002/anie.201304321

19. Naito H, Morisaki Y, Chujo Y. o-Carborane-Based Anthracene: A Variety of Emission Behaviors. Angewandte Chemie-International Edition 2015; 54 (17): 5084–5087. https://doi.org/10.1002/anie.201500129

20. Bae HJ, Kim H, Lee KM, Kim T, Lee YS et al. Through-space charge transfer and emission color tuning of di-o-carborane substituted benzene. Dalton Transactions 2014; 43 (13): 4978–4985. https://doi.org/10.1039/c3dt52465e

21. Duan YC, Pan QQ, Zhao ZW, Gao Y, Wu Y et al. Theoretical Simulations of Thermochromic and Aggregation-Induced Emission Behaviors of a Series of Red-Light Anthracene-o-carborane Derivatives. Chemistry-A European Journal 2021; 27 (37): 9571–9579. https://doi.org/10.1002/chem.202100235

22. Tahaoglu D, Usta H, Alkan F. Revisiting the Role of Charge Transfer in the Emission Properties of Carborane-Fluorophore Systems: A TDDFT Investigation. Journal of Physical Chemistry A 2022; 126 (26): 4199–4210. https://doi.org/10.1021/acs.jpca.2c02435

23. Tanaka K, Gon M, Ito S, Ochi J, Chujo Y. Recent progresses in the mechanistic studies of aggregation-induced emission-active boron complexes and clusters. Coordination Chemistry Reviews 2022; 472. https://doi.org/10.1016/j.ccr.2022.214779

24. Berksun E, Nar I, Atsay A, Ozcesmeci I, Gelir A et al. Synthesis and photophysical properties of a porphyrin-BODIPY dyad and a porphyrin-o-carborane-BODIPY triad. Inorganic Chemistry Frontiers 2018; 5 (1): 200–207. https://doi.org/10.1039/c7qi00608j

25. Huh JO, Kim H, Lee KM, Lee YS, Do Y et al. o-Carborane-assisted Lewis acidity enhancement of triarylboranes. Chemical Communications 2010; 46 (7): 1138–1140. https://doi.org/10.1039/b918263b

26. Nishino K, Yamamoto H, Tanaka K, Chujo Y. Development of Solid-State Emissive Materials Based on Multifunctional o-Carborane-Pyrene Dyads. Organic Letters 2016; 18 (16): 4064–4067. https://doi.org/10.1021/acs.orglett.6b01920

27. Ji L, Riese S, Schmiedel A, Holzapfel M, Fest M et al. Thermodynamic equilibrium between locally excited and charge-transfer states through thermally activated charge transfer in 1-(pyren-2'-yl)-o-carborane. Chemical Science 2022; 13 (18): 5205–5219. https://doi.org/10.1039/d1sc06867a

28. Nishino K, Morisaki Y, Tanaka K, Chujo Y. Electron-donating abilities and luminescence properties of tolane-substituted nido-carboranes. New Journal of Chemistry 2017; 41 (19): 10550–10554. https://doi.org/10.1039/c7nj02438j

29. Kwon S, Wee KR, Cho YJ, Kang SO. Carborane Dyads for Photoinduced Electron Transfer: Photophysical Studies on Carbazole and Phenyl-o-carborane Molecular Assemblies. Chemistry-a European Journal 2014; 20 (20): 5953–5960. https://doi.org/10.1002/chem.201304474

30. Kim SY, Cho YJ, Son HJ, Kim CH, Kang SO. Geometry and steric effects on the electronic states of aryl-o-carboranes. Journal of Organometallic Chemistry 2018; 865: 152–158. https://doi.org/10.1016/j.jorganchem.2018.03.041

31. You DK, Lee JH, Choi BH, Hwang H, Lee MH et al. Effects of Multi-Carborane Substitution on the Photophysical and Electron-Accepting Properties of o-Carboranylbenzene Compounds. European Journal of Inorganic Chemistry 2017 (18): 2496–2503. https://doi.org/10.1002/ejic.201700192

32. Ochi J, Tanaka K, Chujo Y. Experimental proof for emission annihilation through bond elongation at the carbon-carbon bond in o-carborane with fused biphenyl-substituted compounds. Dalton Transactions 2021; 50 (3): 1025–1033. https://doi.org/10.1039/d0dt03618h

33. Nghia NV, Oh J, Sujith S, Jung J, Lee MH. Tuning the photophysical properties of carboranyl luminophores by closo- to nido-carborane conversion and application to OFF-ON fluoride sensing. Dalton Transactions 2018; 47 (48): 17441–17449. https://doi.org/10.1039/c8dt03771j

34. Naito H, Uemura K, Morisaki Y, Tanaka K, Chujo Y. Enhancement of Luminescence Efficiencies by Thermal Rearrangement from ortho- to meta-Carborane in Bis-Carborane-Substituted Acenes. European Journal of Organic Chemistry 2018; 2018 (16): 1885–1890. https://doi.org/10.1002/ejoc.201800151

35. Tu DS, Leong P, Guo S, Yan H, Lu CS et al. Highly Emissive Organic Single-Molecule White Emitters by Engineering o-Carborane-Based Luminophores. Angewandte Chemie-International Edition 2017; 56 (38): 11370–11374. https://doi.org/10.1002/anie.201703862

36. Naito H, Nishino K, Morisaki Y, Tanaka K, Chujo Y. Luminescence Color Tuning from Blue to Near Infrared of Stable Luminescent Solid Materials Based on Bis-o-Carborane-Substituted Oligoacenes. Chemistry-an Asian Journal 2017; 12 (16): 2134–2138. https://doi.org/10.1002/asia.201700815

37. Shin N, Yu S, Lee JH, Hwang H, Lee KM. Biphenyl- and Fluorene-Based o-Carboranyl Compounds: Alteration of Photophysical Properties by Distortion of Biphenyl Rings. Organometallics 2017; 36 (8): 1522–1529. https://doi.org/10.1021/acs.organomet.7b00093

38. Weber L, Kahlert J, Bohling L, Brockhinke A, Stammler HG et al. Electrochemical and spectroelectrochemical studies of C-benzodiazaborolyl-ortho-carboranes. Dalton Transactions 2013; 42 (6): 2266–2281. https://doi.org/10.1039/c2dt32378h

39. Mori H, Nishino K, Wada K, Morisaki Y, Tanaka K et al. Modulation of luminescence chromic behaviors and environment-responsive intensity changes by substituents in bis-o-carborane-substituted conjugated molecules. Materials Chemistry Frontiers 2018; 2 (3): 573–579. https://doi.org/10.1039/c7qm00486a

40. Frisch MJ, Trucks GW, Schlegel HB, Scuseria GE, Robb MA et al. Gaussian 09, Revision A.02. Wallingford CT: Gaussian Inc.; 2009.

41. Zhao Y, Truhlar DG. The M06 suite of density functionals for main group thermochemistry, thermochemical kinetics, noncovalent interactions, excited states, and transition elements: two new functionals and systematic testing of four M06-class functionals and 12 other function. Theoretical Chemistry Accounts 2008; 120 (Meeting on Practicing Chemistry with Theoretical Tools): 215–241. https://doi.org/10.1007/s00214-007-0310-x

42. Walker M, Harvey AJA, Sen A, Dessent CEH. Performance of M06, M06-2X, and M06-HF Density Functionals for Conformationally Flexible Anionic Clusters: M06 Functionals Perform Better than B3LYP for a Model System with Dispersion and Ionic Hydrogen-Bonding Interactions. Journal of Physical Chemistry A 2013; 117 (47): 12590–12600. https://doi.org/10.1021/jp408166m

43. Lu T, Chen FW. Multiwfn: A multifunctional wavefunction analyzer. Journal of Computational Chemistry 2012; 33 (5): 580–592. https://doi.org/10.1002/jcc.22885

44. Xu CY, Li TR, Miao JL, Liu KX, Nie Y et al. Bridged o-carborane-anthracene dyads as dual state emission luminogens: synthesis, characterization, and mechanochromic properties. New Journal of Chemistry 2023; 47 (9): 4448–4456. https://doi.org/10.1039/d3nj00027c

45. Peach MJG, Benfield P, Helgaker T, Tozer DJ. Excitation energies in density functional theory: An evaluation and a diagnostic test. Journal of Chemical Physics 2008; 128 (4). https://doi.org/10.1063/1.2831900